N. Manuchehrabadi

A. Attaluri

Department of Mechanical Engineering,
University of Maryland Baltimore County,
1000 Hilltop Circle,
Baltimore, MD 21250

H. Cai
Department of Physics,
University of Maryland Baltimore County,
1000 Hilltop Circle,
Baltimore, MD 21250

R. Edziah

E. Lalanne

Center for Advanced Studies
in Photonics Research,
University of Maryland Baltimore County,
1000 Hilltop Circle,
Baltimore, MD 21250;
Department of Physics,
University of Maryland Baltimore County,
1000 Hilltop Circle,
Baltimore, MD 21250

C. Bieberich
Department of Biology,
University of Maryland Baltimore County,
1000 Hilltop Circle,
Baltimore, MD 21250

R. Ma
Department of Mechanical Engineering,
University of Maryland Baltimore County,
1000 Hilltop Circle,
Baltimore, MD 21250

A. M. Johnson
Center for Advanced Studies
in Photonics Research,
University of Maryland Baltimore County,
1000 Hilltop Circle,
Baltimore, MD 21250;
Department of Physics,
University of Maryland Baltimore County,
1000 Hilltop Circle,
Baltimore, MD 21250

L. Zhu[1]
Associate Professor
Department of Mechanical Engineering,
University of Maryland Baltimore County,
1000 Hilltop Circle,
Baltimore, MD 21250
e-mail: zliang@umbc.edu

MicroCT Imaging and In Vivo Temperature Elevations in Implanted Prostatic Tumors in Laser Photothermal Therapy Using Gold Nanorods

In this study, in vivo animal experiments are performed on implanted xenograph prostatic tumors in nude mice to investigate enhanced laser energy absorption in the tumors by an intratumoral injection of gold nanorod solutions. in vivo temperature mapping of the tumors during laser photothermal therapy has shown the feasibility of elevating tumor temperatures higher than 50 °C using only 0.1 ml nanorod solution and a low laser irradiance of 1.6 W/cm^2 incident on the tumor surface. The temperature profile suggests that normal tumor tissue still absorbs some amount of the laser energy without nanorod presence; however, the injected nanorods ensure that almost all the laser energy is absorbed and confined to the targeted tumors. The inverse relationship between the temperature elevations and the tumor size implies a relatively uniform spreading of the nanorods to the entire tumor, which is also shown by microcomputed tomography (microCT) imaging analyses. The feasibility of detecting 250 OD gold nanorod solution injected to the tumors is demonstrated via a high resolution microCT imaging system. Compared to other nanostructures, the gold nanorods used in this study do not accumulate surrounding the injection site. The relatively uniform deposition of the nanorods in the tumors observed by the microCT scans can be helpful in future study in simplifying theoretical simulation of temperature elevations in tumors during laser photothermal therapy. [DOI: 10.1115/1.4007161]

Keywords: gold nanorods, laser photothermal therapy, hyperthermia, microCT, nanorod concentration distribution

[1]Corresponding author.
Manuscript received March 23, 2012; final manuscript received May 24, 2012; published online September 24, 2012. Assoc. Editor: Jung-Chih Chiao.

Introduction

In recent years, laser photothermal therapy using gold nanoshells or gold nanorods has emerged as a promising therapeutic method due to its ability to deliver and confine adequate thermal dosage to tumors. By varying the geometric parameters of the nanostructures, gold nanoshells and nanorods can be tuned to have strong absorption and scattering to a specific laser wavelength. The strong absorption is due to optical resonances of gold when its size is much smaller than the visible light wavelength [1,2]. Among a wide range of laser wavelengths, the near infrared (NIR) laser at ~800 nm is one of the most attractive wavelengths to researchers in the field of laser photothermal therapy, due to suggested deep optical penetration in normal tissue. For example, based on previous experimental studies, the attenuation coefficient of an 800 nm wavelength laser in water is approximately $0.1\,cm^{-1}$, which is equivalent to a laser penetration depth of 10 cm in water [3]. Therefore, human tissue, consisting of mostly water, would appear almost "transparent" to the 800 nm laser light before the laser reaches the nanostructures in tumors. The laser energy absorbed in an area congregating by gold nanoshells or nanorods is then transferred to the surrounding tissue by heat conduction. As for a very deep-seated tumor, optical fibers may be used to allow laser irradiation on the tumor surface. Therefore, it has been suggested that this approach not only achieves targeted delivery of laser energy to the tumor, but also maximally concentrates a majority of the laser energy in the tumor region.

The feasibility of using laser photothermal therapy for tumor destruction has been tested both in tissue culture [4–9] and implanted tumors in mice [2,10–13]. Most in vivo experiments performed on mice involved injecting gold nanoshell solutions of approximately 0.1–0.4 ml with concentrations varying from 10^9 to 10^{11} nanoshells per ml solution. Typical laser radiance at the surface was reported starting at $2\,W/cm^2$; however, some researchers stated that $50\,W/cm^2$ was needed for the photothermal therapy to be effective [5,10–13]. Laser spot size was reported varying from 1 to 5 mm in diameter [12,13]. Heating duration could be shorter than several minutes or longer than 15 min [7,12]. Successful treatments have been demonstrated by the shrinkage of the tumors following the laser therapy, as well as by the observed tumor cell death in the tissue culture. A few experiments measured temperatures at one or two tumor locations without temperature mapping of the entire tumor [11]. The large variations in the previous treatment protocols suggested possible variations in the tumor sizes, the nanoshell/nanorod concentrations in the tumors, its interaction with the laser light, as well as local blood perfusion rate in the tumors.

A recent NIR study by Schwartz et al. [14] reported photothermal ablation via systematic delivery of gold nanoshells to an orthotopic tumor in canine models. They compared the real time magnetic resonance imaging (MRI)-derived temperature mappings of canine transmissible venereal tumors in the canine brain models versus normal white and gray matter on the contralateral side of the brain. This study showed that 3.5 W of laser energy resulted in an average temperature of 65.8 °C in the brain exposed to heating of 3 min. Similar experiments were performed by the same group on mice and temperature elevations were larger than 41 °C above the baseline [15]. It has been shown by those two studies that passive accumulation of nanoshells in the tumor sites via systemic delivery was successful. The challenge of systemic delivery is how to deliver nanoshells if the tumor is poorly perfused. An alternative delivery approach, which is the focus of this study, is to directly infuse nanorods into the extracellular space in tumors through micro-infusion. In a few studies using direct nanoshell/nanorod injection to tumors, there is limited information available on how the injection parameters such as the injection amount, nanofluid concentration, and injection rate affect nanostructure deposition and the resulted temperature elevations in the tumors.

For successful cancer treatment, the tumor should be heated with a minimum thermal dosage to induce cell damage, while minimizing overheating in the surrounding healthy tissues. Thus, one of the main challenges for reliable cancer therapy is to precisely control loading and distribution of gold nanorods in targeted tumors [16–19]. Since tumors are opaque, nanostructure distribution in tissue is often studied either by theoretical modeling approaches, or via dye enhanced imaging on superficial layers of tumors [20]. Previous studies [19,21,22] by our group have demonstrated that computer tomography (CT) scan is a promising technique to characterize the distribution of intratumorally injected magnetic nanoparticles in tumors and tissue-equivalent gels. Three-dimensional nanoparticle concentration distribution has been analyzed in those previous studies [19,21,22].

The objectives of this study are to evaluate whether a very small amount of commercially available nanorod solutions can confine laser energy to tumors and induce sufficient temperature elevations in the tumors and to understand nanorod distribution in tumors using microCT imaging technique. In vivo animal experiments were performed on implanted xenograph prostatic tumors in nude mice to measure tumor temperature fields via injecting a very small amount of nanorod solution to the tumors subject to a low laser irradiance on the tumor surface. The effect of nanorod concentration on the steady state temperature elevation distribution along two tumor paths was evaluated. The quantification of the gold nanorod concentration distribution in the implanted prostate tumors was conducted based on reconstructed microCT images of the resected tumors. Since the gold nanorod solution may spread into the entire tumor, correlations among the tumor size, the average microCT grayscale value, and the measured maximal temperature elevation were also investigated.

Experimnetal Method and Materials

Animal and Tumor Models. Fifteen albino, laboratory-bred strain of the house mouse (BALB)/c Nu/Nu male mice (3–6 months old, mean ± SD: 25.84 ± 4.3 g) bearing PC3 xenograft tumors purchased from the National Cancer Center were used in the study. Prostate cancer cell line PC3 cells were grown in a physiological bicarbonate buffering solution (RPMI 1640) and harvested with trypsin digestion. A total of 10^7 PC3 cells were subcutaneously injected via a 26-gauge needle to the right and left flanks of each nude mouse. Flank xenografts were observed within 2–3 weeks after the injection and the tumor size growth was measured via a caliper. Once the inoculated tumors reached a desired size (at least 10 mm in diameter), the mouse was used for the laser experiment. The mouse was anesthetized with sodium pentobarbital solution (40 mg/kg, i.p.). Its body temperature was maintained using a water-jacketed heating pad and was monitored via a thermocouple inserted in the rectum for the entire experiment. The experimental protocol has been approved by the University of Maryland Baltimore County IACUC.

Gold Nanorod Injection. Two concentrations of commercially available gold nanorod solutions (NanPartz™, CO) with an optical density (OD) of 50 and 250 were tested in this study. Seven mice were assigned to the 50 OD group, while the other eight mice were in the 250 OD group. The gold nanorods have an aspect ratio of 4.5 (longitudinal length: 45 nm and transversal diameter: 10 nm). Longitudinal resonance spans at 808 nm while their transverse resonance occurs at about 520 nm. The amounts of nanoparticles per ml for the 50 OD and 250 OD solutions are 3.2×10^{13} and 2.1×10^{14} NPS/cc, respectively. The gold nanorod solution was loaded on a syringe pump with multiple syringe holders (Kd Scientific S230, Holliston, MA). A 26-gauge Hamilton needle (Fischer Scientific, Springfield, NJ) was used for a unilateral injection of 0.1 cc of the gold nanorod solution into the center of one tumor at an infusion rate of 5 μl/min.

Laser Irradiation and Temperature Measurements. After the gold nanorod injection, two fine copper-constantan thermocouples with a wire diameter of 100 μm were inserted into the tumor to map the temperature elevations in the tumor. In order to place the thermocouple in the tumor, a 22 gauge needle was inserted first and went through the center of the spherical tumor all the way to the other end. The thermocouple was inserted into

the needle from one side until it reached the other side. Then, the needle was pull out of the tumor. The second thermocouple was fixed with the same procedures except that it passed the center of the bottom surface of the tumor, which was the interface between the tumor and the mouse body. Another three thermocouples were used for measuring the skin surface, environment, and rectum temperatures. All temperatures were measured and recorded by a thermoreader (Omega DAQPRO-5300, Stamford, CT). The thermocouples have been calibrated following the user's manual of the thermoreader before the experiments and the temperature resolution is nominally 0.05 °C.

The experimental setup is shown in Fig. 1. A two picoseconds, pulsed Tsunami mode-locked laser at 808 nm with the repetition rate of 80 MHz (Spectra Physics Ti: Sapphire laser) was used to irradiate the surface of one tumor for up to 15 min. The laser radiance at the tumor surface was fixed at 1.6 W/cm^2 (an average power of 0.6 W and a laser spot of 7 mm in diameter). After the steady state was established, the temperatures along both tumor tissue paths were measured when one withdrew the thermocouples from their initial positions at an increment of 2 mm until they reached the other end of the tumor tissue path. The thermocouples stayed at each tumor location for 20 s. This time duration is considered much longer than the characteristic time for the thermocouple to approach the same temperature as the tumor. The contralateral tumor was used as the baseline control without nanorod injection. Among the fifteen contralateral tumors, seven tumors were used for the micrCT imaging study described later, while the rest of the contralateral tumors were subject to the same laser irradiance as the one with the nanorod injection. After the heating experiment, the system was turned off and the mouse was removed from the platform. The mouse was euthanized via Na pentobarbital overdose (160 mg/kg, i.p.)

MicroCT Imaging and Image Analysis. We randomly selected seven mice for the microCT imaging study. The tumors of the mice were all injected with the 250 OD gold nanorod solutions. Its contralateral tumors served as a control with neither nanorod injections nor laser irradiance. After the heating experiment, those mice were euthanized and both tumors were surgically resected for microCT scanning. A high resolution microCT system (Skyscan 1172, Microphontonics, PA) (Fig. 2) was used to scan the tumors with or without gold nanorods. Note that all tumors were scanned right after the euthanasia to minimize any variation of time between the nanorod injection and scanning. The tumors were placed in a low density Styrofoam and mounted on a platform inside the imaging system. The acceleration voltage used was 50 kV and the applied current was 200 μA with a 0.5 mm aluminium filter. A medium scanning resolution of 17 μm (pixel size) was selected and the pixel volume was $17 \times 17 \times 17$ μm^3. Since the pixel size is much bigger than the nanorod size, the microCT would not show individual nanorods in the scanned image; however, we expect to see nanorod-induced density increases, based on our preliminary study [21]. The time required to finish the entire scan was approximately 40 min. A total of 500 individual images with an image size of 2000×1000 pixels were obtained for each scanned tumor.

The acquired images from the scan were reconstructed using the NRecon® software package provided by Microphotonics. Artifacts such as beam hardening and ring artifact were minimized in the reconstruction. The reconstruction program takes the projection images as input, and gives the cross section images as output. For all the tumors, the scan parameters and reconstruction parameters were kept the same. Then, the reconstructed images were analyzed using the CTan® software package by Microphotonics. Each greyscale image is represented by pixel index numbers ranging from 0 to 255. Estimation of the tumor volume (mean ± SD: 590 ± 250 mm^3) was performed via selecting the total region of interest (ROI) by interpolating the local ROI (ROI of each slice) throughout the selected tissue region. The CTan® software also allows determination of the percentages of tissue volume containing a specific pixel index number range within the tumors.

Results

Temperature Distribution. The measured steady state temperature distribution profile in the tumors is shown in Fig. 3. The temperature field in the tumor is not uniform. The 250 OD nanorod solution results in much higher temperature elevations (at least 11 °C above its baseline temperature of 37 °C) in the tumor than that induced by the 50 OD nanorod solution. To achieve a minimal temperature elevation of 6 °C (or 43 °C tissue temperature), this figure suggests that the size of the tumor should be smaller than 12 mm in diameter when using the 50 OD nanorod solution.

In principle, the 800 nm laser light appears almost transparent in water [3]. However, tissue does not consist of pure water, and some components inside tumors may have strong absorption and scattering to the 800 nm laser. Figure 4 compares the temperature

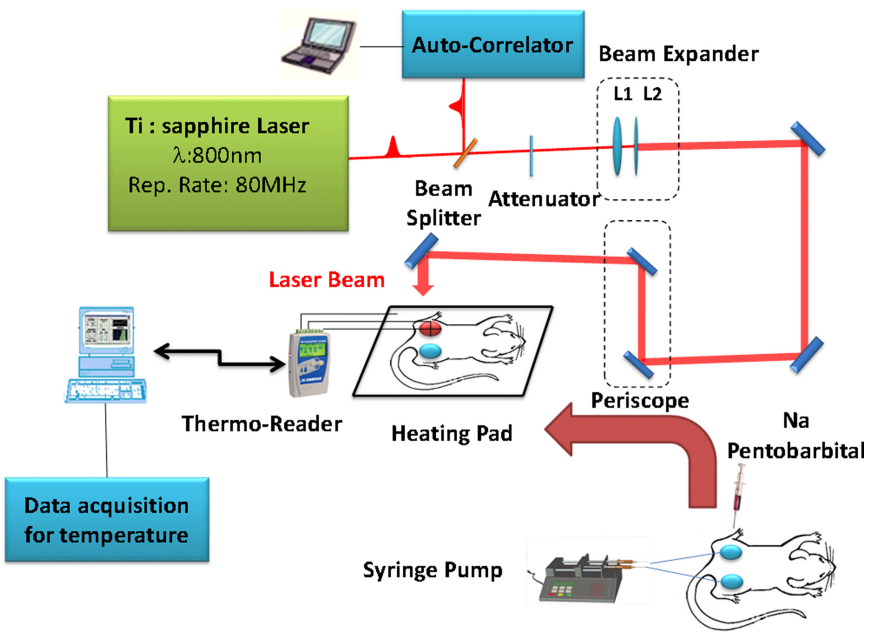

Fig. 1 Experimental setup for the laser heating experiment

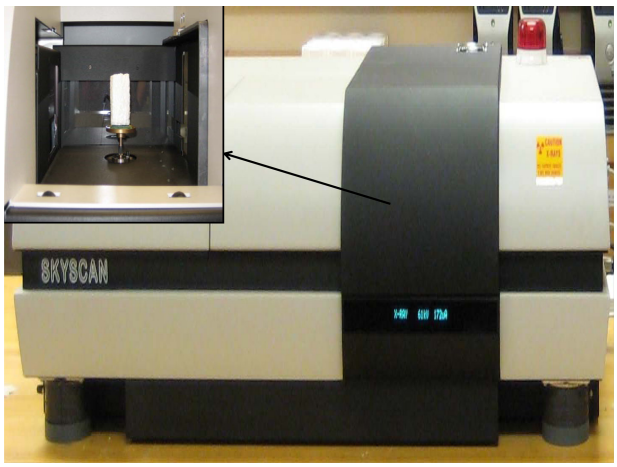

Fig. 2 The SkyScan 1172 microCT imaging system. The inset shows the inner chamber where a sample container is used to hold the specimen.

elevations at the two tumor center locations with or without nanorod injection. Laser absorption by the tumor tissue is evident and it results in 11 °C elevations in the tumor spherical center. On the other hand, temperature elevations from the baseline of 37 °C are 19 °C and 24 °C induced by the 50 OD and 250 OD solutions, respectively. If we assume that the highly concentrated 250 OD solution absorbs 100% of the laser energy, compared to the temperature elevations by the 250 OD solutions, normal tumor tissue absorbs at least 25% (5 °C/20 °C, $T_{max,bottom}$ in Fig. 4) of the laser energy incident on the tumor surface. The result suggests that the tumor tissue is far from "transparent" to the 800 nm lasers. Figure 4 also illustrates the effectiveness of using a less concentrated nanorod solution (50 OD), which results in more than 19 °C temperature elevations at the tumor spherical center. Based on the temperature elevations, one may estimate that approximately 70% (14 °C/20 °C, $T_{max,bottom}$ in Fig. 4) of the laser energy is absorbed by the tumor due to the presence of the 50 OD solution. The measured temperatures at the tumor bottom are much smaller than that at the tumor spherical center, with approximately 4 °C–6 °C lower. This is expected since the laser energy is attenuated when penetrating from the top surface of the tumor to reach the tumor bottom surface.

It is possible that in a larger tumor, the concentration of the nanorods in the tumor is lower, due to spreading of the nanorod

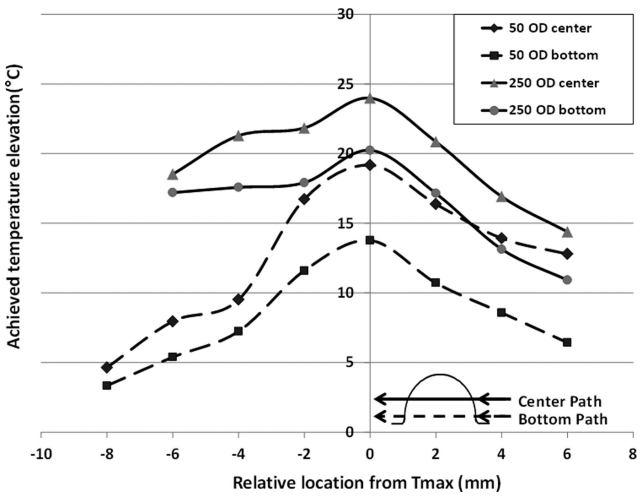

Fig. 3 Steady state temperature elevation profiles in tumors for two different concentrations of gold nanorod solutions. Temperature mappings are along two tumor paths shown on the right bottom of the figure.

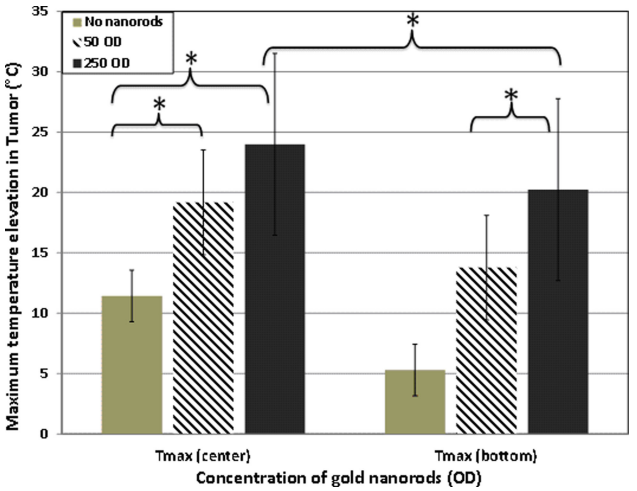

Fig. 4 Maximum temperatures recorded in the tumor centers for two concentrations of gold nanorod solutions during the laser experiment. * represents statistical significance of difference with a *p* value <0.05.

solution in the entire tumor. The relationship between the tumor size and the maximum temperature elevation of the tumors is shown in Fig. 5. This figure establishes an inverse correlation between the tumor size and the maximal temperature measured at the tumor spherical center. It may further be interpreted that the lower nanorod concentration due to spreading in a larger tumor causes less concentrated laser energy absorption, and therefore, resulting in a smaller temperature elevation.

MicroCT Image of Nanorod Distribution. Figure 6 gives cross-sectional grayscale images of a tumor with nanorod injection (up-left) and a control tumor (bottom-left). The distribution of the pixel index number along a spatial line is given on the right side of the figure. Generally, with an increase in the specimen density, the tissue should appear brighter in the microCT images. Visual impression of the grayscale images does not suggest a large chunk of density elevations near the injection site, unlike magnetic nanoparticles in a previous microCT study [18]. It is also not evident from the two images to distinguish the difference of the pixel index numbers between those two tumors. However, the pixel index number profiles indicate that the density in the control tumor without nanorods is relatively uniform. On the other hand, there are some isolated regions in the tumor with nanorods having densities much higher than that in the control tumor. This figure

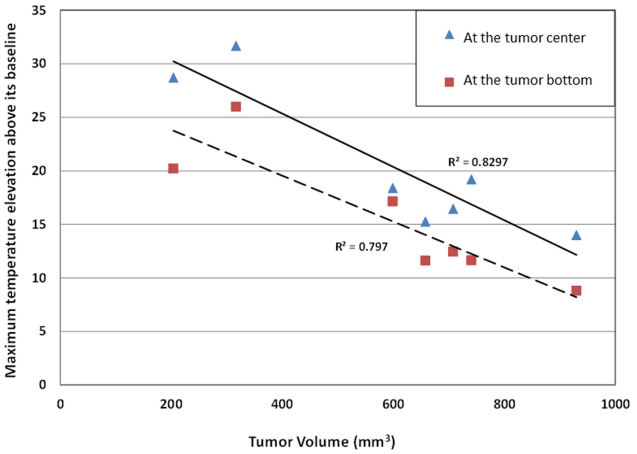

Fig. 5 The relationship between the maximum temperature elevation and the tumor size is represented by symbols. The lines are the linear curve fittings with negative slopes.

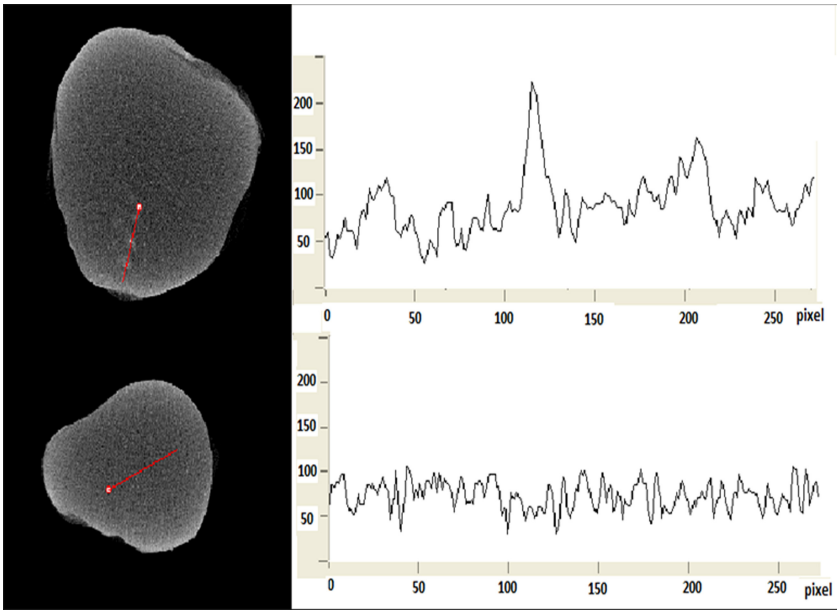

Fig. 6 Gray-scale microCT image of one slice of a tumor with nanorod injection (up-left) and a control tumor (bottom-left). The right side profiles show how the pixel index number varies alone a spatial line.

suggests that gold nanorod solution spreads relatively uniform over the entire tumor. It also demonstrates that the injected nanorods result in a higher local density indicated by the peaks in the index number profiles.

To better understand nanorod-induced density variation in the tumors, we calculate the occupied nanorod distribution volume percentage for different pixel number ranges. The gold nanorod distribution volume represents the total volume of all the pixel volumes containing certain pixel index number ranges. By comparing it to the total tumor volume, one can calculate the distribution volume percentage. Figure 7 plots the distribution volume percentages associated with ten index number ranges. In principle, the grayscale number varies from 0 to 255. The percentage for the range between 200 and 255 is negligible in this study; therefore, it is not included in the figure. The summation of all the percentages for each tumor group should be very close to 100%. Figure 7 is constructed based on the seven mice selected for the microCT study. Clearly, in the control tumor group without nanorods, more than 65% of the tumor region has a pixel index number smaller than 100. In the tumor group with the nanorod injection, only 50% belongs to the same range. It is evident that the injected nanorods shift the distribution volume profile to higher density ranges. 25% of total occupied volume of the tumors in the control group is distributed in the pixel index range between 60 and 80, while only 16.5% in the tumor group with the nanorod injection. In contrast, for the pixel index range of 120–140 that implies higher nanorod concentrations, a higher percentage is seen in the tumor group with the nanorod injection (24% in the injected group vs. 17% in the control group). Based on the profiles, one can calculate the average pixel number of the entire tumor. It has been shown that the average pixel index number is 97 for the control group and 110 for the injected group, showing an overall increase in the material density by the presence of the nanorods.

Figure 8 shows the correlation between the tumor volume and the average pixel index number for the seven tumors with nanorod injections. This inverse relationship accredits our hypothesis that

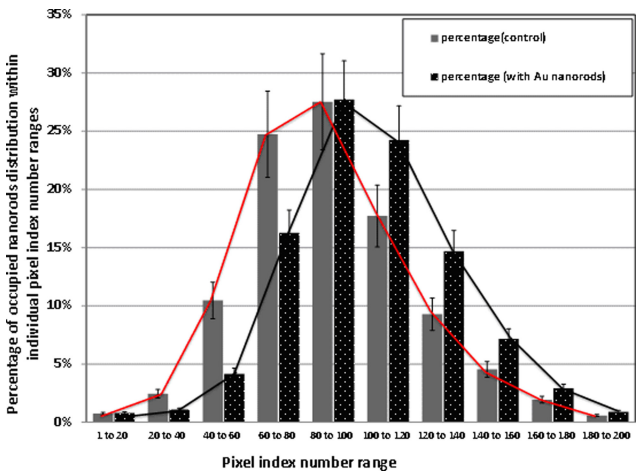

Fig. 7 Percentages of the occupied nanorods distribution within individual pixel index number ranges for the tumor group with gold nanorods and the tumors in the control group.

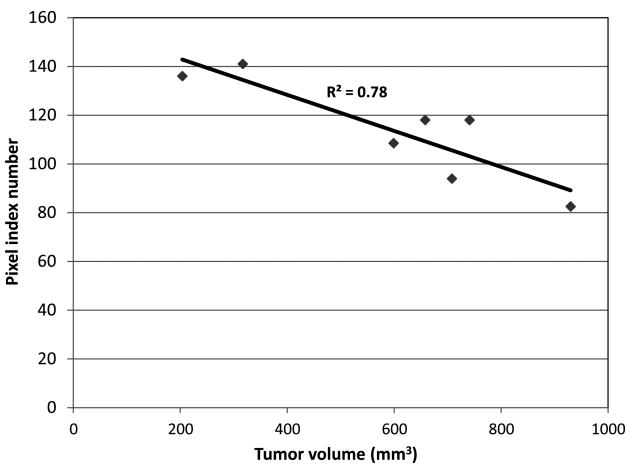

Fig. 8 The inverse relationship between the average pixel index number and the tumor size. The line is the linear curve fitting with a negative slope.

the gold nanorods spread over the entire tumor, rather than accumulating around the injected site. The bigger the tumor size, the more dispersed the gold nanorods in the tumors, and thereby the smaller average pixel index number. This inverse correlation is also consistent with what is illustrated in Fig. 5.

Discussion

Laser photothermal therapy using gold nanorods is a newly developed approach and has been tested in the past several years, and most of the previous studies used systemic delivery of nanoshells or nanorods. In this study, we focused on intratumoral injection of gold nanorod solution to xenograph prostatic tumors in nude mice. One advantage of intratumoral injection versus intravenous injection is the ability to design optimized treatment protocols via using multiple intratumoral nanofluid injection sites to generate sufficient temperature elevations in the entire tumor [23–25]. Since gold nanorods are the major laser energy absorbers in the tumors, nanorod deposition in tumors is crucial in determining whether the entire laser incident on the tumor surface has been absorbed by the tumor and how the laser energy is absorbed along the laser path. In this study, we tested two different concentrations of gold nanorod solutions to get a better idea of tumor temperature field via measuring temperature elevations along two tumor paths. The in vivo temperature field suggests a nonuniform distribution of temperature rises, with a lower temperature elevation at the tumor periphery and on the bottom surface of the tumor. Both the 50 OD and 250 OD nanorod solutions, which are the highest commercially available gold nanorod concentrations provided by the company, achieve up to 17 °C and 24 °C temperature elevations, respectively, after 15 min of laser irradiation. This is much higher than the therapeutic temperature threshold of 43 °C (or 6 °C above the baseline 37 °C) to induce cytotoxic responses with a heating duration longer than one or 2 h [18]. Since tumor temperature may not be uniform, it is important to emphasize possible underheating in tumor periphery. As shown in this study, the 250 OD nanorod solution results in at least 10 °C temperature elevation at the tumor periphery in tumors up to 12 mm in diameter. Using the Arrhenius integral, one may be able to estimate how long the heating time should be to achieve tumor necrosis in the entire tumor. On the other hand, temperatures at the tumor periphery, especially on the bottom of the tumor are lower than 43 °C when the 50 OD nanorod solution is injected into tumors larger than 12 mm in diameter; therefore, the delivered thermal dosage may not be sufficient with a heating duration of only 15 min.

One result of this study is the strong laser energy absorption in tumors without nanorod injection. Laser photothermal therapy was originally proposed to utilize the "optical window" of the spectrum around 800 nm laser wavelength to achieve deep laser energy penetrations in tissue before it reaches the targeted tumor. Similar to previous studies [14,15], our results also suggests that laser energy absorption and/or scattering in tissue should not be neglected. This may be largely due to some components in tissue, such as skin melanin, hemoglobin, etc., which can absorb near infrared laser at 800 nm. In the in vivo experiments using implanted tumors in mice, possible strong blood perfusion rate in the tumors may have contributed to the laser energy absorption without nanorod injections. In future clinical applications of laser photothermal therapy, collateral thermal damage may still occur due the some laser energy absorption by normal tissue.

The experimental measurements of tumor temperatures during heating also implies that tumors alone can only absorb a small percentage of the laser energy, since the achieved temperature elevations with the 250 OD nanorod injection are much higher than that without nanorods. In fact, based on the temperature elevations from its baseline body temperature, one can estimate that normal tumors in this study absorb approximately 25% of the laser energy. This is consistent with a previous theoretical simulation of laser energy absorption in a spherical tumor using Monte Carlo method [26]. In that study, assigning an absorption coefficient and a scattering coefficient of $0.1\,cm^{-1}$ to model a normal tumor, one can determine that only 29% of the incident laser energy on the tumor top surface is absorbed by the tumor. It is evident that the presence of the 250 OD nanorod solutions in the tumors greatly enhances laser energy absorption in the tumors and ensures almost none of the laser energy escapes to the surrounding tissue. The current study uses highly concentrated nanorod solutions comparing to that in the previous studies. It may be the reason that only a very small amount (0.1 ml) of the nanorod solution is needed to achieve irreversible thermal damage when the laser irradiance is very low ($1.6\,W/cm^2$). This may have clinical relevance since it requires a much shorter time for injecting the nanorod solution in a clinical setting. Nevertheless, the 50 OD nanorod solutions are equally good, although it does not confine all the laser energy to the tumor.

MicroCT imaging technique again demonstrates its ability of imaging density increase due to presence of nanostructures in tumors. Our previous study [21] has shown that the 250 OD nanorod solutions can induce sufficient density elevation to be detected by the microCT system, while the microCT system does not illustrate detectable increase in pixel index number induced by the 50 OD nanorod solutions. The 250 OD nanorod solutions has a density slightly higher than the normal tissue density due to its huge amount of nanorods in the solution; therefore, it is used in this study to visualize nanorod concentration distribution in the tumors after the intratumoral injection. Our previous studies using iron based magnetic nanoparticles for cancer treatment have shown bulk accumulation of nanoparticles surrounding the injection sites in the same type of tumors [18]. This is not what we observed in the tumors with nanorods in this study. Compared to the magnetic nanoparticles, the gold nanorods used in this study seem encountering small resistance during the intratumoral injection and spreading to the entire tumor. This is further accredited by the inversed relationship between the tumor size and the measured maximal temperature elevation in the tumors. Another advantage of a relatively uniform nanorod distribution in tumors is in theoretical modeling, which may allow modeling nanorods as a homogeneous distribution in tumors with reasonable accuracy.

In summary, temperature mapping of implanted prostatic tumors in mice during laser photothermal therapy has shown the feasibility of elevating tumor temperatures higher than 50 °C using only 0.1 ml nanorod solution and a low laser irradiance of $1.6\,W/cm^2$ incident on the tumor surface. The temperature profile suggests that normal tumor tissue still absorbs some amount of laser energy without nanorod presence; however, the injected nanorods ensure that almost all the laser energy is confined to the targeted tumors. The inverse relationship between the temperature elevations and tumor sizes implies a relatively uniform spreading of nanorods to the entire tumor, which is also shown by the microCT imaging analyses. The feasibility of detecting 250 OD gold nanorod solution injected to tumors is demonstrated via a high resolution microCT imaging system. Compared to other nanostructures, gold nanorods used in this study do not accumulate surrounding the injection site. The relatively uniform deposition of nanorods in tumors observed by the microCT scans can be helpful for future study in simplifying theoretical simulation in tumors for laser photothermal therapy.

Acknowledgment

This research was supported in part by an NSF research Grant No. CBET-0828728, an NSF MRI Grant No. CBET-0821236 and a research grant from UMBC Research Seed Fund Initiative. The research is performed in partial fulfillment of the requirements for the Ph.D. Degree from University of Maryland Baltimore County (UMBC) by Navid Manuchehrabadi.

References

[1] Lal, S., Clare, S. E., and Halas, N. J., 2008, "Nanoshell-Enabled Photothermal Cancer Therapy: Impending Clinical Impact," Acc. Chem. Res., **41**(12), pp. 1842–1851.

[2] Skrabalak, S. E., Chen, J., Lu, X., Li, X., and Xia, Y., 2007, "Gold Nanocages for Biomedical Applications," Adv. Mater., **19**, pp. 3177–3184.
[3] Reidenbach, H.-D., 2007, "Laser Safety," *Springer Handbook of Laser and Optics*, F. Traeger, ed., Springer, New York.
[4] Bernardi, R. J., Lowery, A. R., Thompson, P. A., Blaney, S. M., and West, J. L., 2008, "Immunonanoshells for Targeted Photothermal Ablation in Medulloblastoma and Glioma: An In Vitro Evaluation Using Human Cell Lines," J. Neuro-Oncol., **86**(2), pp. 165–172.
[5] El-Sayed, I. H., Huang, X., and El-Sayed, M. A., 2006, "Selective Laser Photo-Thermal Therapy of Epithelial Carcinoma Using Anti-EGFR Antibody Conjugated Gold Nanoparticles," Cancer Lett., **239**, pp. 129–135.
[6] Gobin, A. M., Moon, J. J., and West, J. L., 2008, "EphrinAl-Targeted Nanoshells for Photothermal Ablation of Prostate Cancer Cells," Int. J. Nanomed., **3**(3), pp. 351–358.
[7] Melancon, M. P., Lu, W., Yang, Z., Zhang, R., Cheng, Z., Elliot, A. M., Stafford, J., Olson, T., Zhang, J. Z., and Li, C., 2008, "In Vitro and In Vivo Targeting of Hollow Gold Nanoshells Directed at Epidermal Growth Factor Receptor for Photothermal Ablation Therapy," Mol. Cancer Ther., **7**(6), pp. 1730–1739.
[8] Norman, R. S., Stone, J. W., Gole, A., Murphy, C. J., and Sabo-Attwood, T. L., 2008, "Targeted Photothermal Lysis of the Pathogenic Bacteria, Pseudomonas Aeruginosa, With Gold Nanorods," Nano Lett., **8**(1), pp. 302–306.
[9] Whitney, J., Dorn, H., Rylander, C., Campbell, T., Geohegan, D., and Rylander, M. N., 2010, "Spatiotemporal Temperature and Cell Viability Measurement Following Laser Therapy in Combination With Carbon Nanohorns," Proceedings of the ASME Summer Bioengineering Engineering Conference, Naples, FL, June 16–19, ASME Paper No. SBC2010-19619.
[10] O'Neal, D. P., Hirsch, L. R., Halas, N. J., Payne, J. D., and West, J. L., 2004, "Photo-Thermal Tumor Ablation in Mice Using Near Infrared-Absorbing Nanoparticles," Cancer Lett., **209**, pp. 171–176.
[11] Stern, J. M., Stanfield, J., Kabbani, W., Hsieh, J. T., and Cadeddu, J. A., 2008, "Selective Prostate Cancer Thermal Ablation With Laser Activated Gold Nanoshells," J. Urol., **179**, pp. 748–753.
[12] Hirsch, L. R., Stafford, R. J., Bankson, J. A., Sershen, S. R., Rivera, B., Price, R. E., Hazle, J. D., Halas, N. J., and West, J. L., 2003, "Nanoshell-Mediated Near-Infrared Thermal Therapy of Tumors Under Magnetic Resonance Guidance," PNAS, **100**(23), pp. 13549–13554.
[13] Qin, Z., and Bischof, J. C., 2010, "One Dimensional Experimental Setup to Study the Heating of Nanoparticle Laden Systems," Proceedings of the ASME Summer Bioengineering Engineering Conference, Naples, FL, June 16–19, ASME Paper No. SBC2010-19676.
[14] Schwartz, J. A., Shetty, A. M., Price, R. E., Stafford, R. J., Wang, J. C., Uthamanthil, R. K., Pham, K., McNichols, R. J., Coleman, C. L., and Payne, J. D., 2009, "Feasibility Study of Particle-Assisted Laser Ablation of Brain Tumors in Orthotopic Canine Model," Cancer Res., **69**(4), pp. 1659–1667.
[15] Stafford, R. J., Shetty, A., Elliott, A. M., Schwartz, J. A., Goodrich, G. P., and Hazle, J. D., 2011, "MR Temperature Imaging of Nanoshell Mediated Laser Ablation," Int. J. Hyperthermia, **27**(8), pp. 782–790.
[16] Elliott, A. M., Stafford, R. J., Schwartz, J., Wang, J., Shetty, A. M., Bourgoyne, C., O'Neal, P., and Hazle, J. D., 2007, "Laser-Induced Thermal Response and Characterization of Nanoparticles for Cancer Treatment Using Magnetic Resonance Thermal Imaging," Med. Phys., **34**, pp. 3102–3108.
[17] Xie, H., Gill-Sharp, K. L., and O'Neal, D. P., 2007, "Quantitative Estimation of Gold Nanoshell Concentrations in Whole Blood Using Dynamic Light Scattering," Nanomed.: Nanotechnol., Biol., Med., **3**, pp. 89–94.
[18] Attaluri, A., Ma, R., Qiu, Y., Li, W., and Zhu, L., 2011, "Nanoparticle Distribution and Temperature Elevations in Prostatic Tumors in Mice During Magnetic Nanoparticle Hyperthermia," Int. J. Hyperthermia, **27**(5), pp. 491–502.
[19] Feng, Y., Fuentes, D., Hawkins, A., Bass, J., Rylander, M., Elliott, A., Shetty, A., Stafford, R., and Oden, J., 2009, "Nanoshell-Mediated Laser Surgery Simulation for Prostate Cancer Treatment," J. Eng. Comput., **25**, pp. 3–13.
[20] Pluen, A., Boucher, Y., Ramanujan, S., McKee, T. D., Gohongi, T., di Tomaso, E., Brown, E. B., Izumi, Y., Campbell, R. B., Berk, D. A., and Jain, R. K., "Role of Tumor–Host Interactions in Interstitial Diffusion of Macromolecules: Cranial vs. Subcutaneous Tumors," PNAS, **98**, pp. 4628–4633.
[21] Attaluri, A., Manuchehrabadi, N., Ma, R., and Zhu, L., 2011, "Quantification of Nanostructure Distribution in Tissue Using MicroCT Imaging," Proceedings of the ASME Summer Bioengineering Conference, Farmington, PA, June 22–25, ASME Paper No. SBC2011-53182.
[22] Attaluri, A., Ma, R., and Zhu, L., 2011, "Using MicroCT Imaging Technique to Quantify Heat Generation Distribution Induced by Magnetic Nanoparticles for Cancer Treatments," ASME J. Heat Transfer, **133**(1), p. 011003.
[23] Salloum, M., Ma, R., and Zhu, L., 2008, "An In-Vivo Experimental Study of Temperature Elevations in Animal Tissue During Magnetic Nanoparticle Hyperthermia," Int. J. Hyperthermia, **24**(7), pp. 589–601.
[24] Salloum, M., Ma, R., Weeks, D., and Zhu, L., 2008, "Controlling Nanoparticle Delivery in Hyperthermia for Cancer Treatment: Experimental Study in Agarose Gel," Int. J. Hyperthermia, **24**(4), pp. 337–345.
[25] Salloum, M., Ma, R., and Zhu, L., 2009, "Enhancement in Treatment Planning for Magnetic Nanoparticle Hyperthermia: Optimization of the Heat Absorption Pattern," Int. J. Hyperthermia, **25**(4), pp. 309–321.
[26] Chen, Y., Ma, R., and Zhu, L., 2011, "Monte Carlo Simulation of Enhanced Laser Absorption in Tumors With Gold Nanorod Injection," Proceedings of the ASME Summer Bioengineering Conference, Farmington, PA, June 22–25, ASME Paper No. SBC2011-53598.